International Journal for Modern Trends in Science and Technology, 9(05): 770-779, 2023

ISSN: 2455-3778 online
DOI: https://doi.org/10.46501/IJMTST0905132
Available online at: http://www.ijmtst.com/vol9issue05.html

Design and Implementation of a FUZZY-Based Interleaved Boost Converter and Current Source Inverter for Solar PV, Battery Energy Storage System in Motor Drive Application

G Vidyasree[1] | Dr. J. Srinu Naick[2]

[1]Department of Electrical and Electronic Engineering, Chadalawada Ramanamma Engineering College, Tirupati, Andhra Pradesh, India.
[2]Department of Electrical and Electronic Engineering, Chadalawada Ramanamma Engineering College, Tirupati, Andhra Pradesh, India.

To Cite this Article
G Vidyasree and Dr. J. Srinu Naick. Design and Implementation of a FUZZY-Based Interleaved Boost Converter and Current Source Inverter for Solar PV, Battery Energy Storage System in Motor Drive Application. International Journal for Modern Trends in Science and Technology 2023, 9(05), pp. 770-779. https://doi.org/10.46501/IJMTST0905132

Article Info
Received: 12 April 2023; Accepted: 02 May 2023; Published: 22 May 2023.

ABSTRACT

In this paper, we provide a FUZZY-based interleaved boost converter and current source inverter for use in a solar photovoltaic/battery energy storage system's motor drive application. One power electronics topology that makes variable speed drives (VSD) possible is the combination of an interleaved boost converter and a Current Source Inverter (CSI). To simplify the controller design, a fuzzy-based interleaved DC/DC converter is developed in the discontinuous conduction mode (DCM). Saturation of the controller and over current in the inductor are common results of strong signal perturbations. As a result, the article delves into the anti-windup and current limit factors as well. Typical proportional integral (PI) controllers have fixed gains, making them highly sensitive to initial conditions and other input parameter changes. The given controller implements a fuzzy logic controller (FLC) to process the speed error, hence enhancing its performance under both dynamic and steady state settings. For PMSM speed regulation, the speed and the processed output are fed into a PI controller. This configuration makes use of a solar photovoltaic (PV) array and a battery to transform solar energy into usable electricity. Using a 3- current source inverter, the gained energy is put to use turning the PMSM. Using an incremental conductance technique, a DC-to-DC converter in the middle stage is used to boost power production. To speed things up, a PV feed-forward term has been built in. Using MATLAB/Simulink, we simulate this architecture in a variety of environmental settings and observe how it reacts.

KEYWORDS: Current Source Inverter, Boost Converter, Maximum Power Point Tracking, Fuzzy Logic Control, and Photovoltaic Modules

1. INTRODUCTION

Renewable energy sources are becoming a good way to make power, thanks to their many benefits, such as being clean, free, and long-lasting. Without a question, renewable energy will be the main source of power in the years to come. Solar photovoltaic energy is expected to become a popular source of power because it is clean, efficient, and reliable. It can also be used anywhere there is sunlight. Also, there are no mechanical noises or movements because the PV energy components are made of semiconductors. The solar cell has a life span of more than 20 years and can cut down on costs for upkeep and management. The irradiation and temperature of the area around the solar cell make it easy for its output power to change, and it is also not very efficient. So, the power regulation system (PCS), which moves power from the PV array to the load, needs to work well. In general, a single-phase PV PCS has two stages of conversion: a dc-to-dc conversion stage and a dc-to-ac conversion stage. The first stage is the dc/dc converter, which does maximum power-point tracking (MPPT) and makes sure the dc-link voltage stays the same even when there isn't much light. To get the most power out of photovoltaic (PV) systems, you need certain parts, hardware, and software, such as solar trackers, converters, and maximum power point tracking (MPPT). The first section is used to track the sun's movement from east to west, maximizing energy production from photovoltaic (PV) modules the maximum power point tracking (MPPT) and DC-DC converters are then utilized to operate the PV panel at its MPP [1]. Boost converters with an interleaved design can assist the PV system reach the same aim of enhanced conversion efficiency. DC-DC boost converters are commonly used in PV system implementation for regulating and increasing the PV panels' output voltage. significant waves in input current and output voltage, as well as significant stress on switching devices, are only a few of the problems plaguing the DC-DC boost converter [3]. In an interleaved boost converter, two identical boost converters are connected in parallel and run at the same switching frequency but in opposite phases. Ripple cancellation, a reduced peak value, and a high frequency are all advantages of the interleaved boost converter's input current and output voltage waveforms [4]. By developing and analyzing a two-stage boost converter, we are able to circumvent the fundamental issue at many MPPT methods—the slow convergence speed and the oscillation around to MPP during steady state operation—using a novel MPPT algorithm that we recently disclosed in [2]. It is expected that the proposed MPPT technique will reduce power loss and speed up tracking reaction time [2], as it has an excellent performance to monitor MPP with minimal oscillation and a rapid convergence speed. They provide traction power for electric propulsion in trains [7, 8], ships [8], and vehicles [9] and pave the way for more widespread adoption of hybrid and fully electric aircraft (MEA) [5, 6]. Modern variable speed drives excel in terms of efficiency, responsiveness, and overall performance. Certainly, important developments in computational technology over the past three decades or so have had a role in the introduction of cutting-edge PE converters. In low and medium power (from hundreds of W to hundreds of kW) applications, the most common PE converter is the three-phase full-bridge converter, also known as the "workhorse" of the industry. The converter's universal applicability is a result of its high reliability and low maintenance requirements. However, a conditioning period is still needed for the CSI, even when using higher frequency drives. This research aims to address this issue by exploring the possibility of doing away with the pre-stage altogether in the case of applications that run continuously at a higher operating frequency. It is believed that a greater level of adoption of the CSI in the field of VSDs is possible if the requirement for a front-end converter were eliminated. This paper's goal is to do this by introducing a novel input current control strategy that can eliminate the requirement for the converter. Historically, a number of solutions have been offered in literature with the goal of controlling the input current idc. These solutions typically centre on the idea of cancelling and treating the input current's harmonic content. Two inverter stages, a Current Source Rectifier (CSR) that actively regulates the idc current and a six-device Pulse Width Modulation (PWM) CSI, are described as the standard approach for driving an induction machine (IM) in [10]. In [11], a different approach is presented for building a CSI drive.

One of the best things about EVs is that they may potentially recoup part of their lost energy, which can be used to either increase their range or decrease the size of their battery [12]. In addition to regenerative braking, a battery, supercapacitors, fuel cells, and solar panels can

be used to increase the range of an electric vehicle. The energy mix is affected by many variables, including vehicle size, mass, power, traffic circumstances, distance, cost, etc. Thus, it appears that, given the size constraint, using a solar PV panel is a highly viable alternative for an auto-rickshaw. Recent years have seen a proliferation of writings on solar-powered auto rickshaws and e-rickshaws [13–15]. NREL research shows that solar PV module efficiencies have increased from 8.2% to 40.6% [16]. Efficiencies in solar PV modules can be increased, which will hasten the arrival of solar-powered EVs. Most electric vehicles (EVs) that are powered by permanent magnet brushless motors use field oriented control (FOC) and direct torque control (DTC) in their electronic control units. Vector-controlled PMSM drives typically use PI controllers to manage speed and current, but their predefined gain settings are particularly sensitive to variations in model uncertainties, parameters, system disturbances, and load. As a result, the drive's performance suffers throughout a wide range of speeds, which is problematic for EV applications. In order to overcome these difficulties, various nonlinear control and soft computing strategies have been developed in the literature for the motor drive control. These include self-tuned PI controllers, adaptive control, sliding mode control, model predictive control, etc [17]-[19]. The attractiveness of fuzzy logic control (FLC) for the speed controller stems from the fact that it is stable across a wide range of disturbances, much like a nonlinear PI controller with adjusted gains for diverse input conditions. Model predictive controllers (MPCs) have grown in popularity in recent years for hybrid switched systems due to their effectiveness and usability. MPC uses an optimality framework that is flexible enough to account for a wide variety of nonlinearities and real-world constraints in order to accomplish its goals [20]. The feasibility of using MPC for DTC of PMSM in maximum torque per ampere operation and flux weakening operation has been thoroughly investigated in [21], [22]. In this study, a 48V, 3kW surface mounted permanent magnet synchronous motor (SPMSM) drive is controlled by a predictive current controller and a fuzzy logic based speed controller fed by a battery and solar PV array. An active flux-based online, sensorless method is utilized to predict the motor's location and speed, reducing costs while increasing reliability. Accuracy of speed estimates varies between the acceleration region and the steady state zone because of the filter's bandwidth limitations. Fuzzy logic controllers, in contrast to classical controllers, can accommodate uncertain inputs like estimates and measurements. Furthermore, FLC significantly shortens the time to create and execute [23].

2. SYSTEM OPERATION AND DESIGN

This system includes a photovoltaic array, a battery, a DC-DC interleaved Boost converter, a current source inverter (CSI) based on a trio of insulated gate bipolar transistors (IGBTs), a permanent magnet synchronous motor (PMSM), and a motor drive application. To increase the DC/DC boost converter's power handling capacity, a two-phase interlaced is employed. The tiny signal transfer function from the input voltage to the output voltage has one right half plane zero and two poles, which is consistent with the findings for Buck and Boost converters operating in the discontinuous conduction mode (DCM). In order to create a CSI drive for a Permanent Magnet Synchronous Machine (PMSM) without a front-end converter, this study proposes and tests a new control method. The stability of the CSI is first investigated by developing a large-signal model of the infrastructure. Based on the magnitude and direction of the speed error, the FLC makes a correction. The PI controller, which regulates the PMSM's velocity, receives inputs on both the rate of change and the speed error. The provided controller enhances the dynamic and steady-state responses of the PMSM and motor drive application

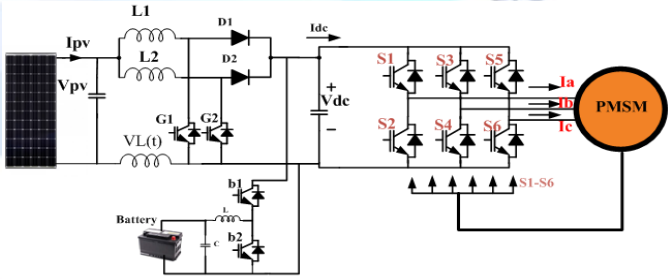

Fig.1 schematic diagram of proposed system

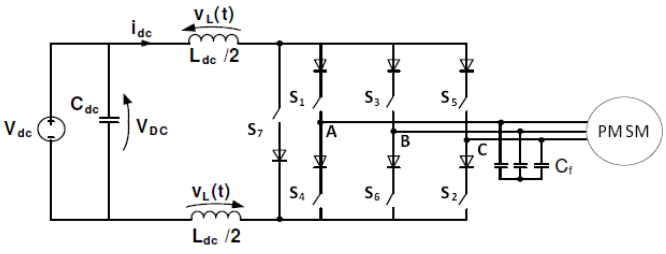

Fig.2 existing system of CSI7

3. PV SYSTEM COMPONENTS ANALYSIS

There are typically three components that make up a PV system, all of which collaborate to convert solar radiation into electricity. The photovoltaic array, or PV cells, are the initial component. The MPP tracker follows the DC-DC converter as the third component. Fig. 3 is a diagram depicting a typical component of a PV system. The input and output resistances of the DC-DC converter are denoted by Rin and Rout. Three subparts make up this section.

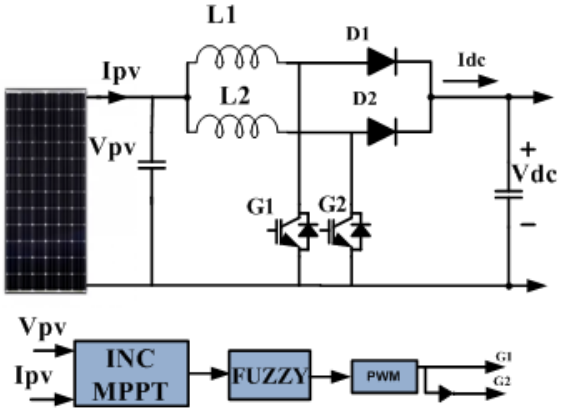

Fig. 3. Complete PV System Schematic.

A. Photovoltaic Cell Model

A PV panel's smallest component is the PV cell. Linear or serial assembly of PV cells yields a PV module, which is then combined into an array. The analogous circuit of a PV cell is depicted in Figure 3; it consists of two resistances and a diode. Metal grid, contact, and current-collecting bus losses are reflected in the series RS resistance. Small leakage currents along the parallel path are represented by the RP resistance, while the diode stands in for the cross current produced by p-n junction semiconductors. Current drawn from a PV cell, denoted Ipv, can be expressed as:

$$I_{PV} = I_G - I_0\left(\exp\left(\frac{q\times(V_{out}+I_{out}\times R_S)}{A\times K\times T}\right)-1\right)-\frac{(V_{out}+I_{out}\times R_S)}{R_P} \quad (1)$$

Furthermore, the PV screen's current output can be mathematically stated as follows:

$$I = N_P \times I_G - N_P \times I_0\left(\exp\left(\frac{q\times(V_{out}+I_{out}\times R_S)}{A\times K\times T\times N_S}\right)-1\right)-N_P\times \frac{(V_{out}+I_{out}\times R_S)}{R_P} \quad (2)$$

The first describes the characteristics of a PV cell model that uses an equivalent circuit. The benefits of the DC-DC interlaced boost converter over the standard boost converter will be discussed in the second. Finally, a quick overview of how the proposed MPPT strategy would function is provided.

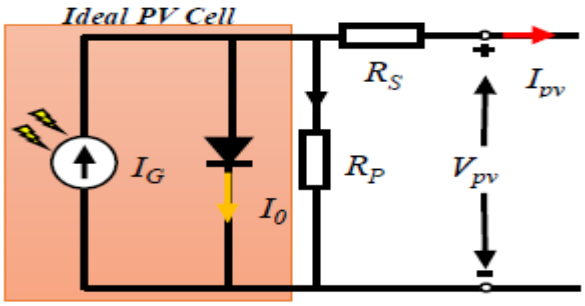

Fig. 4. Equivalent circuit of solar cell.

Where Ipv is the output current of the PV cell, I is the output current of the PV module, IG is the current created by light, I0 is the reverse saturation current, and NP and NS are the number of solar cells connected in parallel and in series, respectively. Boltzmann's constant (k) is 8.65105 eV/K, and the p-n junction temperature (T) is expressed in Kelvin.

B. MPPT

MPPT is obtained using the INC approach in this setup. The operational point is regulated by an INC MPPT technique such that the instantaneous conductance equals the incremental conductance. It provides speedy MPP tracking even in dynamic environments. Because it does not oscillate in a stable state and reacts swiftly to fluctuations, it is useful for solar water pumps. Figure 5 depicts the INC MPPT method's formula. Choosing the right step size is crucial for both static and dynamic performance. The recommended increment for this undertaking is 0.01. In the InC-based MPPT approach, the inputs are the PV array's current (Ipv) and voltage (Vpv), and the governing equations are as follows:

$$\Delta I_{PV} = I_{PV}(k) - I_{PV}(k-1) \quad (3)$$

$$\Delta V_{PV} = V_{PV}(k) - V_{PV}(k-1) \quad (4)$$

$$\frac{\Delta I_{PV}}{\Delta V_{PV}} = \frac{-I_{PV}}{V_{PV}}, \quad \text{at MPP} \quad (5)$$

$$\frac{\Delta I_{PV}}{\Delta V_{PV}} > \frac{-I_{PV}}{V_{PV}} \quad \text{at left of MPP on } P_{PV}\text{-}V_{PV} \text{ curve}$$

Where, P_{PV} is the PV array power

$$\frac{\Delta I_{PV}}{\Delta V_{PV}} < \frac{-I_{PV}}{V_{PV}} \quad \text{at right of MPP on } P_{PV}\text{-}V_{PV} \text{ curve}$$

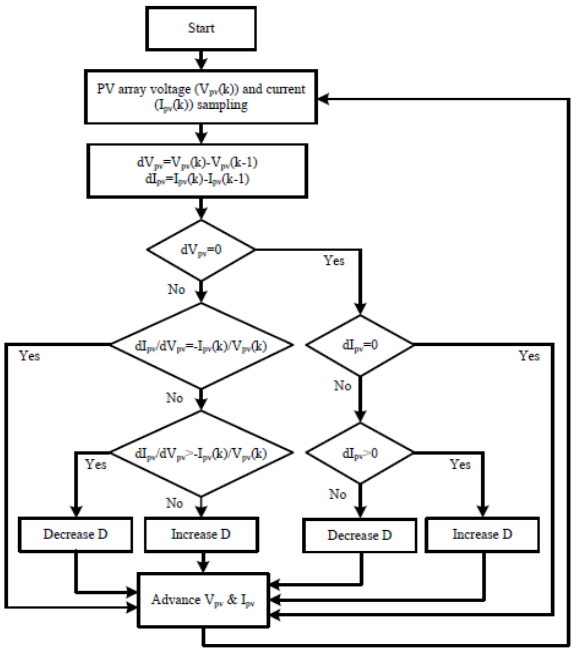

Fig. 5. INC MPPT algorithm.

For (10) to hold, the boost converter's duty ratio must be set via an INC algorithm.

4. INTERLEAVED DC-DC BOOST CONVERTER

A. Circuit Configuration

To better understand the proposed interleaved boost-SEPIC converter, see Figure 6. The illustration shows the boost converter's output connected to the 48V bus and the SEPIC's output connected to the 24V bus.

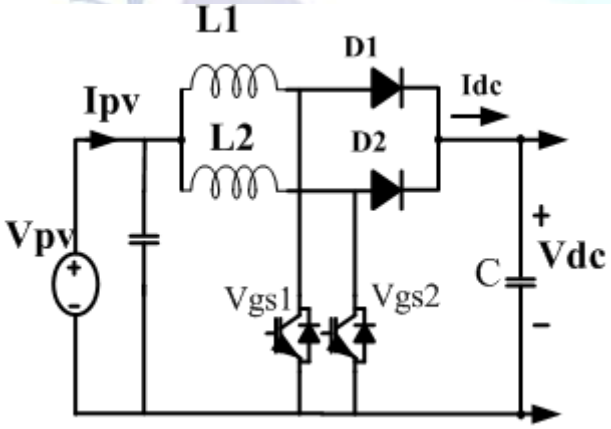

Fig. 6 Circuit diagram of boost- interleaved converter.

It is estimated that the PV (input voltage) can be anywhere from 22V to 28V. For this reason, the 24V bus uses SEPIC while the 48V bus uses a boost converter. By providing gate pulses to S and S2 that are 180 degrees out of phase with one another, the converter is designed to interleave data. The converter operates in CCM mode, with L1 = L2 = L made possible by the design of the source inductors. This single-input, dual-output converter can be put into one of four switching states determined by the positions of switches VgS1 and VgS2. The operation of the circuit in each of these four states is detailed in Table I.

TABLE I

SWITCHING STATES OF BOOST-SEPIC INTERLEAVED CONVERTER

G1	G2	L1	L2	C
0	0	Discharge	Discharge	Charge
0	1	Discharge	charge	Charge
1	0	Charge	Discharge	Charge
1	1	Charge	Charge	Discharge

B. Steady-State Equations

Conversion device shown in Figure 6. Both the VgS1 and VgS2 switches have duty ratios of D1 and D2, respectively. Total output voltage, denoted by Vdc, from the converter. Interactions between output voltages Vdc and input voltage Vpv are described below under steady-state circumstances and during CCM operation:

$$\begin{cases} v_{\mathrm{dc}} = V_{in} \times \frac{\mathrm{D}}{1-D_1} \\ V_{dc} = V_{\mathrm{out}} = V_{pv} \times \frac{1}{1-D_2} \end{cases} \quad (6)$$

If the converter seen in Fig. 6 is implemented in the setup depicted in Fig. 1

To more easily determine how effectively the converter performs and demonstrate that the ripple in the current drawn from the source is as tiny as feasible, it is assumed that the input voltage is V. Simply put:

$$\mathrm{V_{dc}} = \mathrm{V_{out}} = \frac{\mathrm{V_{pv}}}{2} \quad (7)$$

By putting (2) and (3) in place of (1), we can find the steady-state duty ratio of the converter as:

$$D_1 = D_2 = 0.5 \times T_s \quad (8)$$

Figure 3 shows the switching pulses and inductor currents for situations (7) and (8). Since the source inductors and duty cycles of both converters are identical, the ripple current in both converters is also identical [12]. Inductors L1 and L2 have a current ripple that can be detected by:

$$\Delta I_{L1} = \Delta I_{L2} = \frac{V_{in}}{L} \times DT_s \quad (9)$$

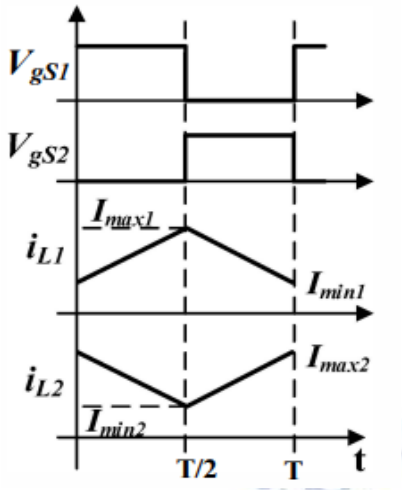

Fig. 7 Steady-state waveforms of the proposed converter.

For switching state 10 and conditions (7) and (8), the inductor currents and source currents are given by:

$$\begin{cases} i_{L1}(t) = \frac{V_{in}}{L} \times t + I_{min}\,1 \\ i_{L2}(t) = -\frac{V_{in}}{L} \times t + I_{max}\,2 \end{cases} \quad (10)$$

$$i_{in}(t) = i_{L1}(t) + I_{L2}(t) = I_{min\,1} + I_{max\,2} \quad (11)$$

For switching state '01' and conditions (3) through (4), the inductor currents and source currents are given by:

$$\begin{cases} i_{L1}(t) = -\frac{V_{in}}{L} \times t + I_{max\,1} \\ i_{L2}(t) = -\frac{V_{in}}{L} \times t + I_{min\,2} \end{cases} \quad (12)$$

$$i_{in}(t) = i_{L1}(t) + I_{L2}(t) = I_{max\,1} + I_{min\,2} \quad (13)$$

Under the assumptions of (7) and (8), we find from (10) and (13) that the theoretical ripple in the current drawn from the source is zero. Similarly, it can be demonstrated that a PV source will have a lower ripple current than a typical, non-isolated converter of the same grade.

5. PROPOSED CONTROL SYSTEM

The fuzzy controls are simple to use. Data entry, analysis, and final results. Input devices such as switches, thumbwheels, etc. are translated into membership functions and truth values at this level. In the processing phase, each rule is executed, a result is generated for each rule, and the results are then combined. The combined result is then converted into a control output at the output stage. While triangles predominate, trapezoids and bell curves are also used as membership functions. More important than the specific geometry is the number and placement of curves. Empirical approaches are the foundation of fuzzy control system design, which is essentially a structured form of trial and error. This is how things usually work: It is important to record the system's inputs and outputs as well as its operational requirements. The inputs' fuzzy sets should be documented. The rules should be written down. Find out how to defuzzify. Go through the test suite to make sure the system works, and change features as needed. Finish the document and let production start.

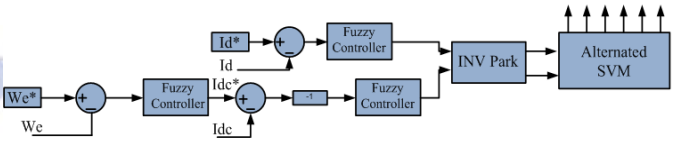

Fig.8 Proposed control strategy with fuzzy based idc current control of a PMSM.

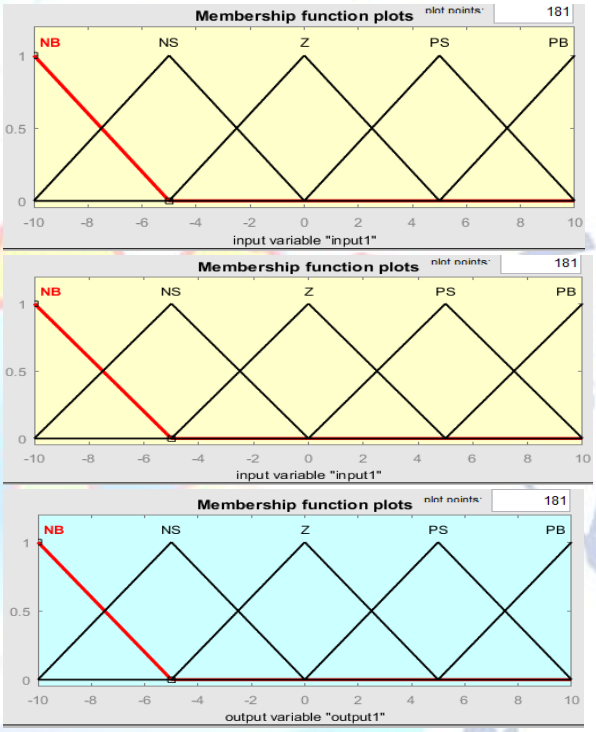

Fig 9 Example figures of input and output membership functions

There are three parts to this device. First, the Inputs are made fuzzy using input membership functions. Rule bases and an inference system are then used to get the final results. The system is then able to make advantage of the clarified fuzzy outputs. The variables selected are error and the rate of change in error. This is how the block model for fuzzy control looks:

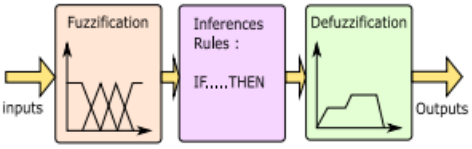

Fig.10 shows the surface generated by the fuzzy system.

Table 1 Inference matrix

de \ e	NB	NS	ZE	PS	PB
NB	NB	NB	NB	NS	ZE
NS	NB	NB	NS	ZE	PS
ZE	NB	NS	ZE	PS	PB
PS	NS	ZE	PS	PB	PB
PB	ZE	PS	PB	PB	PB

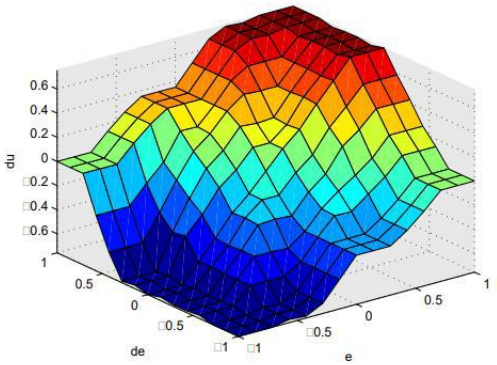

Fig 11 Surface generated by the fuzzy system

Parameters such as language variables, membership functions, inference method and defuzzification strategy must be selected while designing a fuzzy controller for electric motor control. The output of a fuzzy controller is the command itself, whereas the inputs are the error and the error's derivative. As illustrated in Fig.8, the inputs (error, error variation), and the output (input process) are subjected to triangular and trapezoidal membership functions, respectively. The following membership fuzzy subgroups were identified: Negative Big (NB), Negative Small (NS), Zero (ZE), Positive Small (PS), and Positive Big (PB) are the scales used here. In Table 1 we group the fuzzy rules used to map input variables to the controller's output variable.

6. SIMULATION RESULTS

Using the simpower system toolbox in MATLAB/Simulink, we model a solar PV array powered and battery energy storage system PMSM drive application and verify its performance at startup, in steady state, and in dynamic settings such as fluctuating insolation. Starting and steady-state performance are represented together for clarity, whereas dynamic performance is depicted independently. Motor actual currents (iabc), motor speed (N), electromagnetic torque (Te), and DC link voltage (Vdc) are used to evaluate performance alongside insolation (S), solar PV array voltage (Vpv), solar PV array current (Ipv), and solar PV array power (Ppv), state of charge (SOC %), battery current (Ib).

A. System operates in steady state Stable condition

Figure 12 depict the starting and steady-state performance of a solar PV array and a battery PMSM configuration, respectively. Parameters for solar PV show rapid MPP tracking. In less than 0.01 s, the solar PV characteristics stabilise. Since the speed control loop is typically much slower than the current control loop, iabc immediately begins to flawlessly follow iref, but r needs some time to catch up to iref. The rest of the solar PV and motor metrics show a satisfactory response. The DC link voltage has been stabilised at 350 V. At startup, the motor's current consumption is roughly 1.5 times its rated value. It takes longer than 0.1 s for the motor's parameters to stabilise at their steady-state levels. Graphic representation of boost converter parameters is provided. The boost converter's settings likewise behave as predicted.

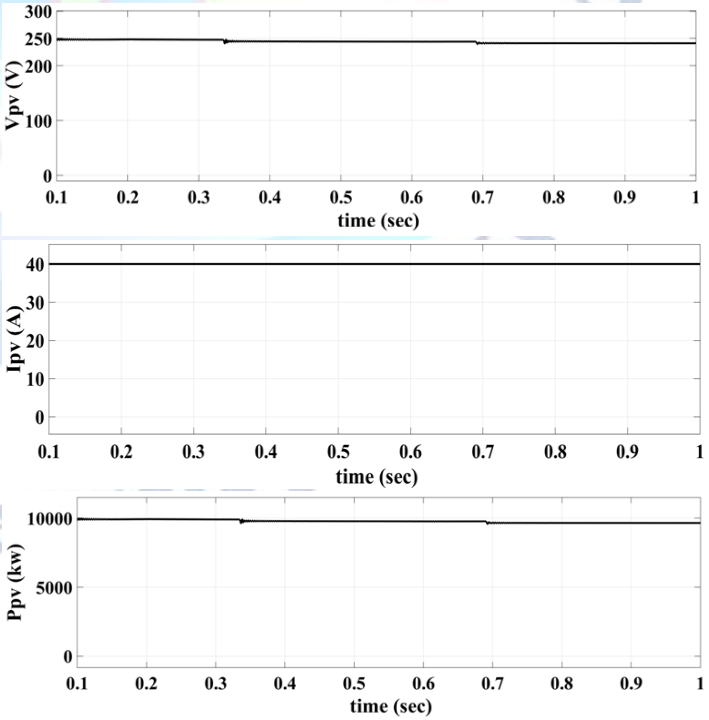

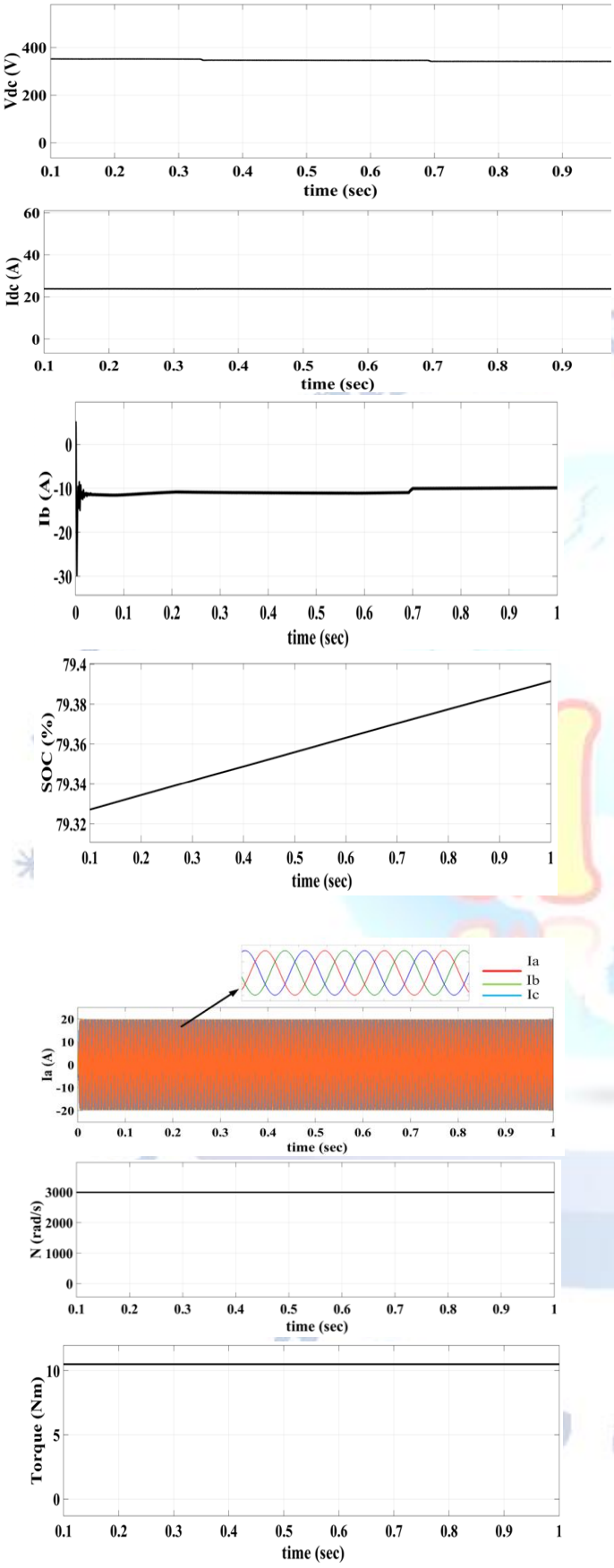

Fig.12 steady state operation of PV, Battery for PMSM drive application

B. Dynamic Performance under Changing Insolation

Figures 13 show how the system behaves dynamically when the amount of sunlight changes while the temperature stays the same. Figure 6(a) shows how the system values change when the amount of sunlight changes from 1000 W/m2 to 0 W/m2 in 0.5 s. The weather, on the other hand, stays the same at 25 C. The change in insolation doesn't change much about Vpv. But it has a big effect on Ipv. Since the number of free electrons created when a photon hits a PN junction and breaks a covalent bond is related to the amount of light hitting the junction from the sun. Ipv drops to almost zero. This cuts the solar PV power to almost nothing compared to what it is rated for. In the same way, the motor factors also change. When the amount of sunlight goes down, r and T also go down. At t = 0.5s and 1s, solar PV arrays may produce less energy, but the batteries attached to the DC link keep the voltage of the DC link at the same level. This is shown in Figure 13. At full power, the PV and battery system cuts down on the amount of sunlight and makes energy. When this isn't enough to meet a load, the battery is drained to meet the load.

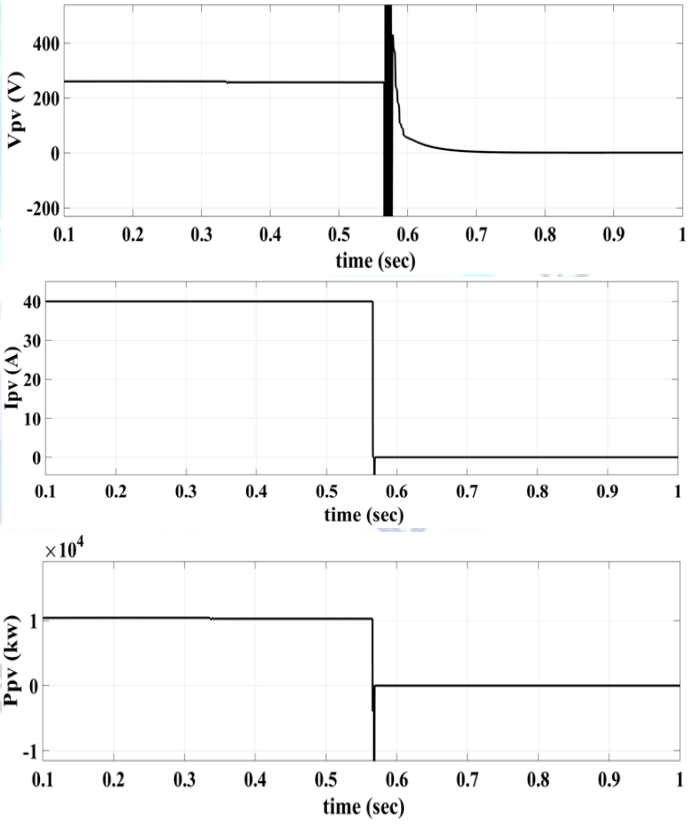

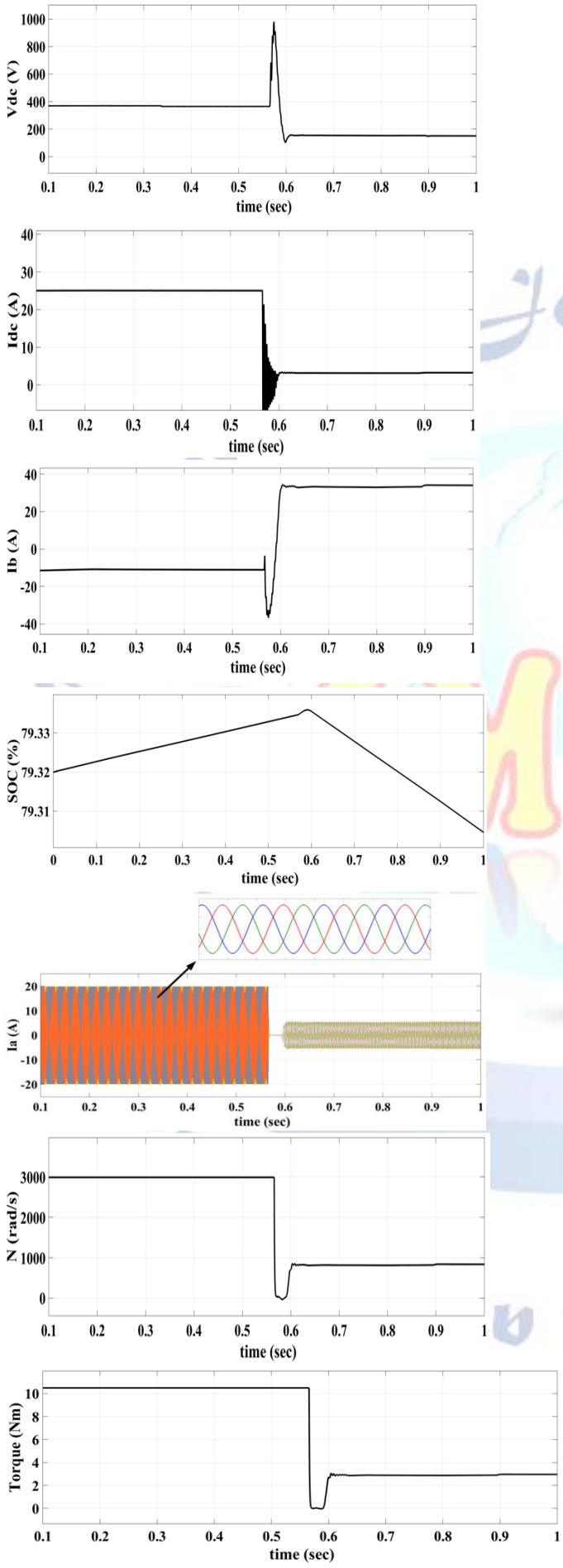

Fig.13 Dynamic performance of PV, Battery system for PMSM drive application

VII CONCLUSION

In the present study, we propose a sensor-free hybrid solar PV battery EV drive setup. By replacing linear PI controllers with the fuzzy-based speed controller and anticipated current controller, drive performance is much improved. The elimination of position monitors also improves the dependability of the drive. By incorporating a stacking boost converter with a novel MPPT method, the output of the PV system is improved in this work. Modelling results for both rapid and gradual changes in solar irradiation demonstrate that the suggested MPPT strategy, which can increase the precision of response time and eliminate oscillations around the MPP in steady state operation, has the best tracking performance. This strategy has been analyzed formally, simulated, and tried in the real world. An investigation of the CSI's stability was performed to learn how well the CSI drive in question performs. This was accomplished by calculating the typical state-space model of the converter and proving its stability under varying conditions of interest by inspecting the location of the eigenvalues. The simulation results demonstrate that the integrated drive is capable of supplying a variable DC link voltage even at high speeds, and that the motor can be maintained in a constant state of lowest copper loss management.

Conflict of interest statement

Authors declare that they do not have any conflict of interest.

REFERENCES

[1] Kamran, M., et al. "Implementation of improved Perturb & Observe MPPT technique with confined search space for standalone photovoltaic system". Journal of King Saud University – Engineering Sciences (2018), https://doi.org/10.1016/j.jksues.2018.04.006.

[2] C. Abdelkhalek, E. B. Said and A. Younes, "A Novel MPPT Tactic for PV Systems with Fast-Converging Speed and Zero Oscillation," 2020 5th International Conference on Renewable Energies for Developing Countries (REDEC), Marrakech, Morocco, Morocco, 2020, pp. 1-6, doi: 10.1109/REDEC49234.2020.9163606.

[3] Mohammed, S. S., & Devaraj, D. (2015, March). Simulation of Incremental Conductance MPPT based two phase interleaved boost converter using MATLAB/Simulink. In 2015 IEEE

International Conference on Electrical, Computer and communication Technologies (ICECCT) (pp. 1-6). IEEE.

[4] Coruh, N., Urgun, S., Erfidan, T., & Ozturk, S. (2011, June). A simple and efficient implemantation of interleaved boost converter. In 2011 6th IEEE Conference on Industrial Electronics and Applications (pp. 2364-2368). IEEE.

[5] G. Buticchi, S. Bozhko, M. Liserre, P. Wheeler, and K. Al-Haddad, "Onboard Microgrids for the More Electric Aircraft - Technology Review,"IEEE Transactions on Industrial Electronics, 2019.

[6] C. Gerada, M. Galea, and A. Kladas, "Electrical Machines for Aerospace Applications," in 2015 IEEE Workshop on Electrical Machines Design, Control and Diagnosis (WEMDCD), March 2015, pp. 79–84.

[7] C. Zhao, D. Dujic, A. Mester, J. K. Steinke, M. Weiss, S. Lewdeni-Schmid, T. Chaudhuri, and P. Stefanutti, "Power Electronic Traction Transformer—Medium Voltage Prototype," IEEE Transactions on Industrial Electronics, vol. 61, no. 7, pp. 3257–3268, July 2014.

[8] T. Ericsen, N. Hingorani, and Y. Khersonsky, "Power electronics and Future Marine Electrical Systems," IEEE Transactions on Industry Applications, vol. 42, no. 1, pp. 155–163, Jan 2006.

[9] D. Gerada, X. Huang, C. Zhang, H. Zhang, X. Zhang, and C. Gerada, "Electrical Machines for Automotive Electrically Assisted Turbocharging," IEEE/ASME Transactions on Mechatronics, vol. 23, no. 5, pp. 2054–2065, Oct 2018.

[10] Y. W. Li, M. Pande, N. R. Zargari, and B. Wu, "DC-Link Current Minimization for High-Power Current-Source Motor Drives," IEEE Transactions on Power Electronics, vol. 24, no. 1, pp. 232–240, 2009.

[11] H.-C. Chen and H.-H. Huang, "Design of buck-type current source inverter fed brushless DC motor drive and its application to position sensorless control with square-wave current," IET Electric Power Applications, vol. 7, no. 5, pp. 416–426, 2013.

[12] B. Berman, "Battery Powered Regenerative SCR Drive," IEEE Transactions on Industry Applications, vol. IA-8, no. 2, pp. 190-194, Mar. 1972.

[13] P. Mulhall, M. Naviwala, S. M. Lukic, J. Braband and A. Emadi, "Entrepreneurial Projects Program at Illinois Institute of Technology: Solar/Battery Hybrid Three-Wheel Auto Rickshaw for India," 2007 IEEE Vehicle Power and Propulsion Conference, Arlington, TX, 2007, pp. 682-689.

[14] K. S. Reddy, S. Aravindhan, and T. K. Mallick, "Techno-Economic Investigation of Solar Powered Electric Auto-Rickshaw for a Sustainable Transport System", Energies ,vol. 10, pp. 754, 2017.

[15] P. Mulhall, S. M. Lukic, S. G. Wirasingha, Y. Lee and A. Emadi, "Solar- Assisted Electric Auto Rickshaw Three-Wheeler," IEEE Transactions on Vehicular Technology, vol. 59, no. 5, pp. 2298-2307, Jun 2010. doi: 10.1109/TVT.2010.2045138

[16] "Champion Photovoltaic Module Efficiency Chart" [Online]. Available: https://www.nrel.gov/pv/module-efficiency.html [Accessed: 18-Apr-2019].

[17] D. Xu, B. Wang, G. Zhang, G. Wang and Y. Yu, "A review of sensorless control methods for AC motor drives," CES Transactions on Electrical Machines and Systems, vol. 2, no. 1, pp. 104-115, March 2018.

[18] D. Liang, J. Li, R. Qu and W. Kong, "Adaptive Second-Order Sliding- Mode Observer for PMSM Sensorless Control Considering VSI Nonlinearity," IEEE Transactions on Power Electronics, vol. 33, no. 10,pp. 8994-9004, Oct. 2018.

[19] X. Zhang, L. Zhang and Y. Zhang, "Model Predictive Current Control for PMSM Drives With Parameter Robustness Improvement," IEEE Transactions on Power Electronics, vol. 34, no. 2, pp. 1645-1657, Feb.2019.

[20] J. Rodriguez and P. Cortes. Predictive control of power converters and electrical drives. Vol. 40. John Wiley & Sons, 2012.

[21] M. Preindl and S. Bolognani, "Model Predictive Direct Torque Control With Finite Control Set for PMSM Drive Systems, Part 1: Maximum Torque Per Ampere Operation," IEEE Transactions on Industrial Informatics, vol. 9, no. 4, pp. 1912-1921, Nov. 2013

[22] M. Preindl and S. Bolognani, "Model Predictive Direct Torque Control With Finite Control Set for PMSM Drive Systems, Part 2: Field Weakening Operation," IEEE Transactions on Industrial Informatics, vol. 9, no. 2, pp. 648-657, May 2013.

[23] P. Vas. Artificial-intelligence-based electrical machines and drives: application of fuzzy, neural, fuzzy-neural, and genetic algorithm-based techniques. vol. 45. Oxford university press, 1999.